# Electrostatics and the Membrane Association of Src: Theory and Experiment†

Diana Murray,‡ Luz Hermida-Matsumoto,§ Carolyn A. Buser,‡,|| James Tsang,‡ Catherine T. Sigal,§,⊥ Nir Ben-Tal,▽,# Barry Honig,▽ Marilyn D. Resh,§ and Stuart McLaughlin*,‡

*Department of Physiology and Biophysics, State University of New York at Stony Brook, Stony Brook, New York 11794-8661, Cell Biology and Genetics Program, Memorial Sloan-Kettering Cancer Center, New York, New York 10021, and Department of Biochemistry and Molecular Biophysics, Columbia University, New York, New York 10032*

*Received August 13, 1997; Revised Manuscript Received November 20, 1997*

ABSTRACT: The binding of Src to phospholipid membranes requires both hydrophobic insertion of its myristate into the hydrocarbon interior of the membrane and nonspecific electrostatic interaction of its N-terminal cluster of basic residues with acidic phospholipids. We provide a theoretical description of the electrostatic partitioning of Src onto phospholipid membranes. Specifically, we use molecular models to represent a nonmyristoylated peptide corresponding to residues 2−19 of Src [nonmyr-Src(2−19); GSSKSKPKDPSQRRRSLE-$NH_2$] and a phospholipid bilayer, calculate the electrostatic interaction by solving the nonlinear Poisson−Boltzmann equation, and predict the molar partition coefficient using statistical thermodynamics. The theoretical predictions agree with experimental data obtained by measuring the partitioning of nonmyr-Src(2−19) onto phospholipid vesicles: membrane binding increases as the mole percent of acidic lipid in the vesicles is increased, the ionic strength of the solution is decreased, or the net positive charge of the peptide is increased. The theoretical model also correctly predicts the measured partitioning of the myristoylated peptide, myr-Src(2−19); for example, adding 33% acidic lipid to electrically neutral vesicles increases the partitioning of myr-Src(2−19) 100-fold. Phosphorylating either serine 12 (by protein kinase C) or serine 17 (by cAMP-dependent protein kinase) decreases the partitioning of myr-Src(2−19) onto vesicles containing acidic lipid 10-fold. We investigated the effect of phosphorylation on the localization of Src to biological membranes by expressing fusion constructs of Src's N terminus with a soluble carrier protein in COS-1 cells; phosphorylation produces a small shift in the distribution of the Src chimeras from the plasma membrane to the cytosol.

The v-Src oncoprotein ($pp60^{v-src}$)[1] and its normal cellular homologue c-Src ($pp60^{c-src}$) are membrane-bound, nonreceptor tyrosine kinases (*1*−*4*). The N terminus of Src contains two motifs essential for membrane localization: a myristate attached cotranslationally to the N-terminal glycine by *N*-myristoyltransferase (*5*−*9*) and a stretch of hydrophilic amino acids rich in positively charged residues (*10*, *11*). Mutations that either prevent myristoylation (*12*−*14*) or reduce the net positive charge in the N-terminal cluster of basic residues (*10*, *11*) inhibit the association of Src with the plasma membrane, producing nontransforming phenotypes.

Studies with either the intact Src protein (*11*) or myristoylated peptides corresponding to the N terminus of Src (*15*) support the hypothesis that the myristate inserts hydrophobically into the hydrocarbon interior of the bilayer and the basic residues interact electrostatically with acidic phospholipids. Myristate alone provides barely enough energy to attach the peptide or protein to membranes (*16*−*18*); the myristate and basic residues act synergistically (or with apparent cooperativity) to effect the membrane binding of Src. For example, adding 33% acidic lipid to electrically neutral vesicles increases the membrane binding of both Src and the N-terminal peptide myr-Src(2−16) (myristate-GSSKSKPKDPSQRRR-$NH_2$) by 3 orders of magnitude (*11*, *15*).

Buser et al. (*15*) described the synergism between Src's two membrane binding motifs with a "ball and string" model that represents the myristoylated peptide or protein as two dimensionless binding sites, A (acyl chain) and B (basic residues), joined by a flexible, electrically neutral string of length *r*. Following Crothers and Metzger (*19*) and Perutz

† This research was supported by Grant MCB-9419175 from the NSF and Grant GM-24971 from the NIH to S.M., Grant BE235 from the American Cancer Society and Grant CA-72309 from the NIH to M.D.R., Grant MCB-9304127 from the NSF and Grant MCA95C015 from the NCSA to B.H., Grant 5T32 NSO 7372-03 from the NIH and a Helen Hay Whitney Foundation Postdoctoral Fellowship to D.M., and the Cancer Research Fund of the Damon Runyon-Walter Winchell Foundation Fellowship to C.A.B.

* Address correspondence to this author. Telephone: 516-444-3039. Fax: 516-444-3432. E-mail: smcl@informatics.informatics.sunysb.edu.

‡ State University of New York at Stony Brook.

§ Memorial Sloan-Kettering Cancer Center.

|| Present address: Cancer Research Department, Merck and Co., West Point, PA 19486.

⊥ Present address: Laboratory of Cellular and Molecular Recognition, National Institute of Mental Health, Bethesda, MD 20892.

▽ Columbia University.

# Present address: Department of Biochemistry, Tel Aviv University, Ramat Aviv 69978, Israel.

[1] Abbreviations: c-Src, $pp60^{c-src}$; CD, circular dichroism; PKA, cAMP-dependent protein kinase; DAG, diacylglycerol; EPR, electron paramagnetic resonance; $\beta$-Gal, $\beta$-galactosidase; LUV, large unilamellar vesicles; myr, myristoylated; nonmyr, nonmyristoylated; PC, phosphatidylcholine; PG, phosphatidylglycerol; PH, pleckstrin homology; $PIP_2$, phosphatidylinositol 4,5-bisphosphate; PS, phosphatidylserine; PKC, protein kinase C; SUV, sonicated unilamellar vesicles; v-Src, $pp60^{v-src}$.

S0006-2960(97)02012-6 CCC: $15.00 
Published on Web 02/06/1998

(*20*), the synergism is treated as a local concentration enhancement effect;[2] once the myristate chain has partitioned into the membrane, the flexible string serves as a tether that confines the basic cluster to a hemisphere of radius $r$ above the membrane, a region of higher lipid concentration. $K_A$ ($M^{-1}$) is the molar partition coefficient that describes the binding of myristoylated N-terminal Src peptides to electrically neutral phospholipid vesicles; it can be interpreted as a measure of the hydrophobic interaction. $K_B$ ($M^{-1}$) is the molar partition coefficient that describes the binding of nonmyristoylated Src peptides to vesicles containing acidic phospholipid; it can be interpreted as a measure of the electrostatic interaction. The ball and string model describes the overall binding as

$$K \approx \frac{3\alpha}{2r} K_A K_B \qquad (1)$$

where $K$ ($M^{-1}$) is the molar partition coefficient that describes the binding of myristoylated Src peptides to vesicles containing acidic phospholipid; $3/(2r)$ describes the coupling between A and B (i.e. it is the ratio of the membrane surface area, $\pi r^2$, and the solution volume, $^2/_3\pi r^3$, that are accessible to the basic cluster when the acyl chain is bound); and $\alpha$ ($=4\text{nm}/M^{-1}$) is a constant that depends only on the surface area per phospholipid (see ref *15* for details). This model's predictions agree qualitatively with measurements of the partitioning of myristoylated Src(2−16) onto phospholipid vesicles (*15*). The model also predicts that synergism between hydrophobic and electrostatic interactions produces strong membrane binding of a peptide corresponding to the C terminus of K-Ras 4B (GKKKKKKSKTKC-farnesyl) (*21*, *22*).

Although the ball and string model accounts for the synergism between hydrophobic and electrostatic interactions, it is descriptive rather than predictive. Specifically, the model requires experimental determination of $K_A$ and $K_B$, and it assumes the two binding sites are dimensionless points connected by an electrically neutral string; this assumption is unrealistic because the basic residues of Src(2−19) are distributed over a distance of about 50 Å (see Figure 1). We have developed a more realistic model that predicts the electrostatic component of the membrane binding of peptides corresponding to the N terminus of Src and describes the synergism between the hydrophobic and electrostatic interactions. We represent the peptide and membrane in atomic detail and the aqueous phase as a continuum solvent (*24*, *25*). We first calculate the electrostatic free energy of interaction between the peptide and membrane using classical electrostatic theory and then derive the molar partition coefficient from the electrostatic results using statistical thermodynamics. Our model extends previous theoretical work that describes the membrane binding of simple basic peptides (*26*) and small basic toxins of known structure (*27*); it is the first application of the methodology to a biologically important protein.

[2] Gelb and co-workers (*22*) discuss alternative treatments that invoke the loss of translational and rotational degrees of freedom [e.g. Page and Jencks (*23*)] that occur upon membrane binding of an acylated or prenylated peptide. Uncertainty about changes in the peptide chain configurational entropy complicates application of these treatments to the membrane partitioning of myristoylated peptides (*22*).

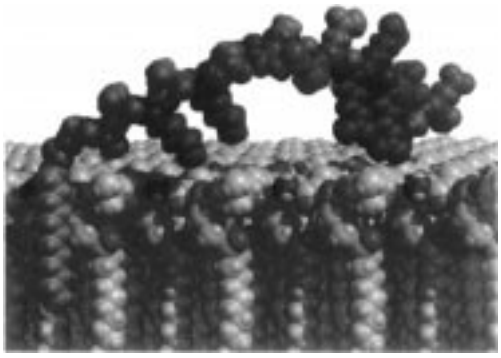

FIGURE 1: Molecular model of the N-terminal region of Src interacting with the upper leaflet of a 2:1 PC/PS bilayer. The front portion of the bilayer has been removed to expose the myristate. The 18-residue peptide (myristate-GSSKSKPKDPSQRRRSLE-$NH_2$) is shown in an extended conformation. The six basic residues are blue, and the two acidic residues are red; the serines phosphorylated by protein kinase C (serine 12) and cAMP-dependent protein kinase (serine 17) are green, and the $CH_2$ groups of the myristate are gold. In the bilayer, PS is identified by its exposed nitrogen (blue); oxygen is red and phosphorus yellow, and carbon and hydrogen are gray.

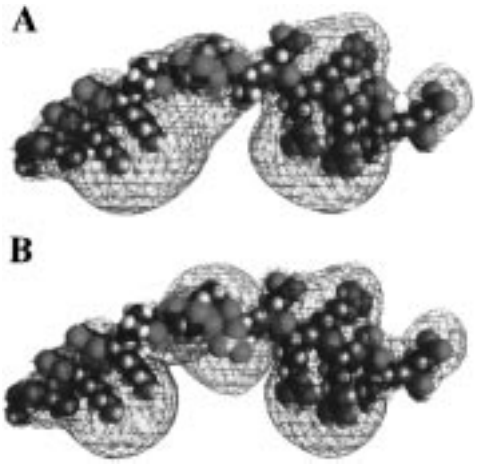


FIGURE 2: Effect of phosphorylation on the electrostatic potential adjacent to Src(2−19). Electrostatic potentials were calculated in a 100 mM monovalent salt solution. The peptides are shown in a configuration similar to that in Figure 1. Three-dimensional equipotential contours are shown at 25 mV (blue mesh) and −25 mV (red mesh). The figures were generated using GRASP (*55*): (A) unphosphorylated Src(2−19), net charge of +5; and (B) Src(2−19) phosphorylated at serine 12, net charge of +3. The phosphate group is identified by its yellow phosphorus.

The N-terminal region of Src contains two serine phosphorylation sites (ref *28* and references therein); serine 12 is phosphorylated by protein kinase C (PKC), and serine 17 is phosphorylated by cAMP-dependent protein kinase (PKA) (see Figure 1). Our model provides an explanation, at the molecular level, for the reduced affinity of phosphorylated Src peptides for membranes: phosphorylation of either serine reduces the net charge of the basic cluster, altering its electrostatic potential (Figure 2) and weakening its electrostatic binding to membranes containing acidic lipids. Although our previous studies used Src(2−16), here we use Src(2−19), which allows us to examine the effect of phosphorylation at either site. While the biological consequence of phosphorylation is controversial, two studies suggest that N-terminal phosphorylation may play a role in translocation of Src from the plasma membrane to the cytosol or cytoskeleton (*29*, *30*).

The studies reported here have four objectives. The first is to calculate the electrostatic component of the membrane binding of nonmyristoylated (nonmyr) Src(2−19) (GSSKSKP-KDPSQRRRSLE-$NH_2$) using atomic models. We compared the theoretical predictions with experimental measurements of the dependence of membrane binding on the ionic strength of the solution and the mole percent of acidic lipid in the vesicles. The second objective is to account for the apparent cooperativity between Src's two membrane binding motifs, the N-terminal myristate and cluster of basic residues, using atomic models. We compared the model's predictions to measurements of the partitioning of myristoylated (myr) Src-(2−19) onto phospholipid vesicles. The third objective is to account for the effect of phosphorylation on the binding of myr-Src(2−19). We compared the model's predictions with measurements of the partitioning of phosphorylated myr-Src(2−19) onto phospholipid vesicles containing 33% acidic lipid. The fourth objective is to study the role of N-terminal phosphorylation on reversible binding of Src to biological membranes. We used chimeric constructs containing the Src N terminus fused to soluble carrier proteins to study the localization of phosphorylated and nonphosphorylated protein in vivo.

## MATERIALS AND METHODS

### *Experiment*

*Materials.* The zwitterionic lipid 1-palmitoyl-2-oleoyl-*sn*-glycero-3-phosphocholine (PC) and the acidic lipids 1-palmitoyl-2-oleoyl-*sn*-glycero-3-phosphoglycerol (PG) and 1-palmitoyl-2-oleoyl-*sn*-glycero-3-phosphoserine (PS) were purchased from Avanti Polar Lipids (Alabaster, AL). Radiolabeled 1,2-di[1-$^{14}$C]oleoyl-L-3-phosphatidylcholine ([$^{14}$C]-PC; specific activity of 100−124 mCi/mmol) was purchased from Amersham (Arlington Heights, IL). Adenosine 5′-triphosphate (ATP) was purchased from Sigma (St. Louis, MO) and $\gamma$-$^{32}$P-radiolabeled adenosine 5′-triphosphate tetra-(trimethylammonium) salt ([$^{32}$P]ATP, specific activity of 3000 Ci/mmol) from NEN Life Sciences Products (Boston, MA). Protein kinase C (PKC) was obtained from Boehringer Mannheim (Indianapolis, IN) and Calbiochem Novabiochem (San Diego, CA), cAMP-dependent kinase (PKA) from Sigma, and 1,2-dioleoyl-*sn*-glycerol (DAG) from Avanti Polar Lipids.

The $NH_2$-terminal sequence (residues 2−19) of myristoylated Schmidt-Ruppin A v-Src and avian c-Src, myr-GSSKSKPKDPSQRRRSLE-$NH_2$, contains six basic residues and two acidic residues. Myristoylated and nonmyristoylated peptides corresponding to residues 2−19 [denoted myr-Src-(2−19) and nonmyr-Src(2−19), respectively] were synthesized with an amide-blocked C terminus to >95% purity as determined by analytical HPLC (Center for the Analysis and Synthesis of Macromolecules, State University of New York at Stony Brook) and used without further purification. F-MOC-myristoylated glycine was purchased from Novabiocehm and used in the synthesis of myr-Src(2−19) without special treatment. Stock solutions at 5 mg/mL peptide were prepared in dimethyl sulfoxide. All aqueous solutions were prepared with 18 MΩ $H_2O$ (Super-Q, Millipore, Bedford, MA) that was subsequently bidistilled in an all-quartz still.

The tritiated myristoylated peptide $^3$H-myr-Src(2−19) was prepared enzymatically as described in ref *7* using purified yeast *N*-myristoyltransferase (*31*). $^3$H-myr-Src(2−19) was purified by HPLC over a $CH_3CN$ gradient (buffer A = $H_2O$ and 0.1% TFA, and buffer B = $CH_3CN$ and 0.1% TFA) on a C18 reverse-phase column; the myristoylated peptide eluted at 45:55 $H_2O$:$CH_3CN$ and 0.1% TFA. The measured activity of $^3$H-myr-Src(2−19) was 0.07 $\mu$Ci/mL.

*PKC Phosphorylation of Myr-Src(2−19).* The reaction mixture contained 20 mM MOPS, 200 $\mu$M $CaCl_2$, 5 mM $MgCl_2$, 50 $\mu$M PC/PS/DAG (62:33:5) sonicated unilamellar vesicles (SUV), 10 $\mu$M Src(2−19), and 50 $\mu$M ATP with a trace of [$^{32}$P]ATP. The PC/PS/DAG SUV were prepared as follows. The lipid mixture in $CHCl_3$, with a trace amount of [$^{14}$C]PC, was initially evaporated under argon and then vacuum-dried for 1 h in a 33 °C water bath. The dried lipid was resuspended in 100 mM KCl and 1 mM MOPS at pH 7; the air was displaced with argon. The lipid solution was then sonicated four times for 10 min in a $H_2O$ bath kept between 15 and 30 °C. Large vesicles were pelleted by centrifugation at 100000*g* for 1 h at 25 °C. The supernatant containing the SUV was used within 24 h.

The phosphorylation reaction was started by the addition of 0.5 $\mu$L of PKC and 1 mM DTT, the solution incubated for 5−60 min at 30 °C, and the reaction terminated with 10 mM EDTA. The reaction mixture was diluted 10-fold in 100 mM KCl, 1 mM MOPS (pH 7), and 0.0065% Triton X-100 and centrifuged at 80000*g* for 1 h at 25 °C. The supernatant was used as a source of PKC-phosphorylated Src(2−19) without further purification. The binding of PKC-phosphorylated myr-Src(2−19) to 2:1 PC/PS LUV was the same for two SUV concentrations (25 nM peptide/0.1 $\mu$M SUV and 50 nM peptide/0.2 $\mu$M SUV), suggesting that the presence of SUV did not affect peptide binding to LUV. The percentage of peptide bound in the membrane partitioning experiments was determined by spotting the peptide on a P81 Whatman filter (Fischer Scientific, Pittsburgh, PA). Control samples containing the same phosphorylation reaction mixture in the absence of peptide were prepared to subtract the contribution from non-peptide-bound $^{32}$P. The filters were washed two times in 0.4% phosphoric acid and transferred to scintillation vials; 100 $\mu$L of 0.001% TX-100 and 3 mL of scintillation fluid were added to each for scintillation counting.

*PKA Phosphorylation of Myr-Src(2−19).* The reaction mixture contained 20 mM MOPS, 5 mM $MgCl_2$, 10 $\mu$M myr-Src(2−19), and 50 $\mu$M ATP with a trace of [$^{32}$P]ATP. The phosphorylation reaction was started by the addition of 2.5 mg/mL PKA (from a stock solution at 10 mg/mL in 20% glycerol and 30 mM DTT), the mixture incubated for 5−30 min at 30 °C, and the reaction terminated with 1 mM EDTA. The reaction mixture was diluted 10-fold in 100 mM KCl, 1 mM MOPS (pH 7), 0.0065% Triton X-100 and centrifuged at 80000−100000*g* for 1 h at 25 °C. The supernatant was used as the source of PKA-phosphorylated Src(2−19) without further purification.

*Sucrose-Loaded Vesicle-Binding Assay.* Sucrose-loaded vesicles resuspended into salt buffer (the internal sucrose concentration is adjusted to be isosmotic with the external salt buffer) were prepared as described by Buser et al. (*15*). In the membrane-binding assay, peptide was mixed with the sucrose-loaded LUV; [peptide] ≪ [lipid] so that the peptide did not bind a significant fraction of the acidic lipid. After 15 min of equilibration at room temperature (22 °C), vesicle-

bound peptide was separated by centrifugation (for 1 h at 100000*g* and 25 °C). Ninety percent of the supernatant and pellet was measured by either a fluorescamine assay for nonradiolabeled peptide, scintillation counting for $^{3}$H-myr-Src(2−19), or P81 filter assay followed by scintillation counting for $^{32}$P-phosphorylated Src(2−19). The fluorescamine assay and the tritium scintillation counting are described by Buser et al. (*15*). The binding of the $^{32}$P-phosphorylated Src(2−19) was determined by spotting 100 $\mu$L of the supernatant and pellet on the respective P81 filters and washing and/or scintillation counting the filters as described above. The fraction of phosphorylated peptide bound to LUV ($f_b$) was determined by deconvolution of the [$^{32}$P]Src(2−19) and the [$^{14}$C]PC radiolabels: $f_b = 1 - [^{32}\text{P-(supernatant)}/[^{32}\text{P(supernatant)} + ^{32}\text{P(pellet)}]]$. Calculations of the percentage of bound peptide were corrected for the 1−8% lipid that remained in the supernatant. Lipid loss was negligible when [lipid] $\geq 10^{-7}$ M. We added 0.0001% Triton X-100 to the solution to prevent unbound myr-Src(2−19) from spinning down during the binding assay to 2:1 PC/PG or 2:1 PC/PS lipids. We observed the same binding of $^{3}$H-myr-Src(2−19) to 2:1 PC/PG LUV at both 0.0001% and 0.0005% Triton X-100, suggesting that this concentration of detergent does not affect peptide binding. In control experiments, the binding of myr-Src(2−19) to PC vesicles was unaffected over the range of Triton X-100 concentrations from 0 to 0.0065%.

For technical reasons, we used the acidic lipid PG rather than PS for the vesicle binding measurements of nonmyr- and myr-Src(2−19). (Fluorescamine reacts with primary amines; thus, we avoid using amine-containing lipids such as PE and PS in the fluorescamine assay described above.) Previous measurements show that simple basic peptides bind with identical affinities to vesicles formed from either PG or PS (*32*). The theoretical calculations (see below) used bilayers constructed from molecular models of PC and PS because PS is the major acidic lipid in mammalian biological membranes.

*Monolayer Adsorption Measurements.* We used an apparatus designed by Fromherz (*33*) to determine directly if nonmyr-Src(2−19) penetrates the phospholipid monolayer when it adsorbs to the surface. The instrument consists of a Wilhemy plate for monitoring the surface pressure of the monolayer and a feedback circuit for maintaining the surface pressure at a constant value. Peptides and other ligands that penetrate the monolayer increase the area, whereas nonpenetrating peptides do not (*26*, *34*, *35*). The monolayers were formed from 1-palmitoyl-2-oleoyl-*sn*-glycero-3-phosphocholine (PC) and 1-palmitoyl-2-oleoyl-*sn*-glycero-3-phosphoglycerol (PG) over a solution containing 0.1 M KCl and 1 mM MOPS at pH 7 with a *T* of 25 °C.

*Circular Dichroism (CD).* Spectra were recorded on a J-20 spectropolarimeter (JASCO, Tokyo, Japan) using a 1 mm cylindrical cell. SUV containing either PC or PG were prepared by ultrasonication (*36*) in buffer containing 0.1 M KCl, 2.5 mM $K_2HPO_4$, and 2.5 mM $KH_2PO_4$ (pH 7).

*Plasmid Constructions*. The Src20$\beta$Gal fusion was created in two steps. Fragments containing the sequence coding for the first 20 amino acids of Src were generated by PCR from a v-Src clone in pGEM3z. The sense primer for all constructs contained a 5′ *Xba*I site and the nucleotide sequence starting 243 bases upstream from the v-Src ATG start site (5′GCTCTAGACACGCTTTTGCATATGATACATAA3′). The antisense primer for the wild-type Src20-$\beta$Gal included the codons for v-Src amino acids 13−20 plus a 3′ *Bam*HI site (5′GCGGGATCCGGCTCCAGGCTGCGCCGGCGCTG3′). Antisense primers for the Src mutants were as follows (with mutations underlined): Src20S12A, 5′ GGATCCGGCTCCAGGCTGCGCCGGCGCTGAGCGGGGTCC3′; Src20S17A, 5′GGATCCGGCTCCAGAGCGCGCCGGCGCTGGCTGGGGTCC3′; and Src20S12A/S17A, 5′GGATCCGGCTCCAGAGCGCGCCGGCGCTGAGCGGGGTCC3′. The PCR products were digested with *Xba*I and *Bam*HI and ligated in-frame to *Xba*I/*Bam*HI-cut pVALO (*37*), a eukaryotic expression vector containing $\beta$-galactosidase under the control of the $\beta$-globin promoter. Similarly, oligonucleotide-directed PCR mutagenesis was used to generate serine to alanine mutations at positions 12 (S12A), 17 (S17A), or 12 and 17 (S12A/S17A) of Src 20 fused to $\beta$-galactosidase.

*Cell Culture, Transfections, and Protein Analyses.* COS-1 cells were maintained in Dulbecco's Minimum Essential Medium (GIBCO catalog no. 121-00061)/10% fetal bovine serum. Transfections were carried out by the DEAE-dextran method in 10 cm Petri dishes according to published protocols (*38*). Twenty-four hours after transfection, cells were split (1:2) to generate duplicate plates. Forty-eight hours after transfection, cells were starved for 1 h in media lacking phosphate and then labeled for 3 h with $^{32}$P-orthophosphate (3000 Ci/mmol, NEN) at a final concentration of 0.4 mCi/mL. At the time of labeling, we added the following cell-permeable phosphatase inhibitors to a final concentration of 0.1 $\mu$M: okadaic acid and calyculin A (Gibco) and cypermethrin and tautomycin (Calbiochem). Labeled cells were harvested and fractionated by hypotonic lysis (*39*) to generate S-100 and P-100 fractions. The following protease inhibitors were included in the lysis buffer: AEBSF (10 $\mu$g/mL), aprotinin (1.5 $\mu$g/mL), pepstatin A (1.5 $\mu$g/mL), leupeptin (1.5 $\mu$g/mL), TLCK (10 $\mu$g/mL), TPCK (10 $\mu$g/mL), benzamidine (10 $\mu$g/mL), and E-64 (1.5 $\mu$g/mL).

The S-100 fraction was adjusted to 1× RIPA buffer [radioimmunoprecipitation assay buffer, 50 mM Tris (pH 8.0), 150 mM NaCl, 1% NP-40, 0.5% deoxycholate, and 0.1% SDS] and immunoprecipitated as follows. One microliter (2 $\mu$g) of anti-$\beta$Gal monoclonal antibody (Promega) was added to samples adjusted to 500 $\mu$L of RIPA and incubated at 4 °C for 3−12 h. Immune complexes were adsorbed to formalin-fixed *Streptomyces aureus* for 20 min at 4 °C and processed as described previously (*39*). The P-100 fraction was resuspended in 1× RIPA buffer and the insoluble material removed by centrifugation at 100000*g* for 15 min followed by immunoprecipitation as above. Immune complexes were washed three times with ice-cold RIPA, denatured in sample buffer, and resolved by SDS−PAGE on 8% gels. Following transfer to Immobilon P−PVDF membranes (Millipore), the transfected protein was detected by Western blotting using the ECL method (Amersham). Western blot membranes were then bleached by light irradiation and re-exposed to film to generate an autoradiograph. Blots and autoradiographs were scanned using an Epson Twain scanner and the images quantitated with Fuji Macbass.

*Theory*

*Determination of K from Experimental Measurements.* We use a molar partition coefficient, *K*, to describe the partitioning of Src(2−19) onto phospholipid membranes (*16*).

*K* ($M^{-1}$) is the proportionality factor between the mole fraction of peptide bound to the membrane, $\chi$, and the molar concentration of peptide free in the bulk aqueous phase, [P]:

$$\chi = \frac{[P]_m}{[L] + [P]_m} = K[P] \quad (2)$$

where $[P]_m$ is the molar concentration of peptide bound to the membrane and [L] is the concentration of lipid accessible to the peptide. The square brackets denote molar concentrations, i.e. the moles of a species divided by the total solution volume. Previous work showed that Src(2−12) does not permeate LUV (*15*); this should be true for Src(2−19) as well because residues 13−19 are hydrophilic. Hence, the peptides bind only to the outer surface of the vesicles, and [L] is approximately $^1/_2$ of the total lipid concentration for these unilamellar vesicles. For all our measurements, [L] $\gg [P]_m$, and eq 2 may be written as

$$[P]_m = K[P][L] \quad (3)$$

The total molar concentration of Src(2−19) in the solution, $[P]_{tot}$, is the sum of bound and free peptide concentrations:

$$[P]_{tot} = [P]_m + [P] \quad (4)$$

Combining eqs 3 and 4, we obtain an expression for *K* as a function of known ([L]) and measured ($[P]_m/[P]_{tot}$) quantities:

$$\frac{[P]_m}{[P]_{tot}} = \frac{K[L]}{1 + K[L]} \quad (5)$$

If we plot the fraction of bound peptide, $[P]_m/[P]_{tot}$, as a function of accessible lipid concentration, [L] (Figures 3A and 4A), we can determine the value of *K* from a least-squares fit of eq 5 to the data (Figures 3B and 4B). Note that when $[P]_m/[P]_{tot} = ^1/_2$, $K = 1/[L]$; i.e. the molar partition coefficient is the reciprocal of the accessible lipid concentration that binds one-half of the total peptide.

Although, we use the word "binding" in this report, "partitioning" is a more accurate definition of the phenomenon we are studying (*40*); our use of eq 3 to determine *K* from experimental data makes no assumption about the specific nature of the interaction. Thus, while eqs 3 and 5 have the same form as the limiting version of a mass action equation for a 1:1 complex, we do not assume a specific, 1:1 interaction between a peptide and a lipid. Previous work has shown that the binding of model peptides to membranes depends only weakly on the chemical nature of either the basic residues (arginine vs lysine) or the monovalent acidic lipid (PS vs PG) (*26*). In contrast, the binding of the multivalent acidic lipid phosphatidylinositol 4,5-bisphosphate ($PIP_2$) to the pleckstrin homology (PH) domain of phospholipase C-$\delta_1$ is highly specific (*41*); e.g. this PH domain binds 10-fold more strongly to 2:1 PC/PS membranes when they contain 3% $PIP_2$ (*42*). As described in detail below, the nonmyristoylated peptides measured as "bound" in our experiments partition onto the membrane through nonspecific electrostatic interactions and may be located an appreciable distance (e.g. 5 Å) from the membrane surface (see, e.g., Figure 1 of ref *26*).

*Gibbs Surface Excess.* Our aim is to calculate *K* for Src(2−19) and compare the theoretical predictions with experimental results. We first provide an overview of the theoretical calculation by considering an oversimplified model for the electrostatic interaction based on Gouy−Chapman theory (*43*), which represents the peptide as a point charge of valence $+Z$, the membrane as a uniformly charged surface, and the monovalent salt ions as point charges. The principles are valid for the more realistic model of the peptide/membrane system we use in our calculations (see Appendix I).

A membrane containing a mixture of neutral and acidic phospholipids attracts counterions (e.g. $K^+$) to and repels co-ions (e.g. $Cl^-$) from its surface. The electrostatic attraction of the counterions is balanced by their statistical tendency to diffuse away from the region of higher concentration, which results in an ionic atmosphere adjacent to the membrane surface (the diffuse double layer). In the linearized version of Gouy−Chapman theory, the electrostatic potential decays exponentially as a function of distance from the membrane surface, *R*:

$$\phi(R) = \phi(0) \exp(-\kappa R) \quad (6)$$

where $\phi$ is the electrostatic potential, *R* is the coordinate normal to the membrane surface, and $1/\kappa$ is the Debye length ($1/\kappa = 10$ Å in a 100 mM monovalent salt solution). Basic peptides added to the aqueous phase are attracted by the negative electrostatic potential, which results in an excess concentration of peptide near the membrane surface relative to that in the bulk solution. The basic peptide concentration is low compared to the monovalent salt concentration. The monovalent cations, and not the basic peptide, are the counterions to the acidic lipids and ensure overall electroneutrality of the system. The concentration, [P(*R*)], of a $+Z$-valence peptide a distance *R* from the membrane surface is

$$[P(R)] = [P(\infty)] \exp[-W(R)/kT] \quad (7)$$

where $[P(\infty)]$ is the peptide concentration in the bulk solution, $W(R)$ is the free energy change that occurs when the peptide moves from the bulk solution to a distance *R* from the membrane, and *k* is the Boltzmann constant. In the linearized Gouy−Chapman theory, $W(R)$ is simply the product of the charge of the peptide, $eZ$ (*e* is the electron charge), and the electrostatic potential, $\phi(R)$. For a 2:1 PC/PS membrane in a 100 mM KCl solution, Gouy−Chapman theory correctly predicts the electrostatic potential is approximately −60 mV at the surface, −20 mV 10 Å (one Debye length) from the surface, and −8 mV 20 Å (two Debye lengths) from the surface (*44*). Gouy−Chapman theory also predicts that at $R = 10$ Å the concentration of a $Z = +5$ peptide is enriched 80-fold with respect to the bulk peptide concentration; our more realistic model (see below) predicts the concentration of nonmyr-Src(2−19) ($Z = +5$) is enriched 30-fold at $R =$ 10 Å. Note that the "extra" peptide ions 10 Å from the surface are defined as bound even though they do not physically contact the membrane; they are measured as bound ions in equilibrium dialysis and sucrose-loaded vesicle measurements.

The Gibbs surface excess (*45*), $\Gamma$, represents the number of moles of peptide adsorbed per unit area of membrane surface. It is calculated by integrating the excess peptide concentration over the distance, $R$, from the membrane [see Figure 1 of Ben-Tal et al. (*26*)]:

$$\Gamma = \int_0^\infty dR\,([P(R)] - [P(\infty)]) \tag{8}$$

The concentration of membrane-bound peptide, $[P]_m$, is given by

$$[P]_m = \frac{A\Gamma}{V} \tag{9}$$

where $A$ is the surface area of membrane accessible to the peptide and $V$ is the volume of the solution. Note that $A/V = A_L N[L]$ where $A_L$ is the surface area occupied by one lipid in the membrane, $N$ is Avogadro's number, and [L] is the accessible lipid concentration (see ref *26* for more details). Combining eqs 3 and 7−9 [and identifying [P] in eq 3 with [P(∞)] in eqs 7 and 8], we obtain an expression for the molar partition coefficient as a function of the free energy of interaction between the peptide and membrane:

$$K = A_L N \int_0^\infty dR\,[\exp[-W(R)/kT] - 1] \tag{10}$$

Thus, if we know the free energy of interaction, $W(R)$, we can calculate the Gibbs surface excess and obtain a theoretical binding constant to compare with experimental measurements (*26*).

*Theoretical Model for Nonmyristoylated Peptides*. Gouy−Chapman theory, which assumes the peptide (a dimensionless point) does not perturb the potential produced by the membrane (a surface of uniformly smeared charge), does not provide an adequate representation of Src(2−19) interacting with a bilayer (see Figure 1). We use a more realistic theoretical model (refs *26* and *27* and Appendix I) to calculate the electrostatic interaction between the peptide and the membrane. Our model accounts for the finite size of the molecules as well as for the reciprocal effects of the peptide and membrane on each other's potentials.

We built atomic models for the peptide and membrane as described in Molecular Models of Src(2−19) and Phospholipid Membranes below. The peptide is docked in the aqueous phase above the membrane. Assigning atomic radii and partial charges to the coordinates of the constituent atoms characterizes the shape and charge distribution of the molecules. We calculate the electrostatic free energy of interaction, $W_B$ (B for basic), by numerically solving the nonlinear Poisson−Boltzmann equation for the peptide/membrane system (ref *26* and Appendix I). Because we do not treat the peptide as a point (Figure 1), we must calculate $W_B$ for many orientations of the peptide with respect to the membrane and average over these orientations at each distance $R$. This produces the six-dimensional generalization of eq 10 (*26*):

$$K = A_L N \int_0^\infty dR\,\langle \exp[-W_B(x,y,R,\theta,\mu,\varphi)/kT] - 1\rangle \tag{11}$$

where the broken brackets denote the average over orientations at each $R$. The coordinates $x$, $y$, $R$, $\theta$, $\mu$, and $\varphi$ locate the peptide with respect to the membrane. $x$ and $y$ are translations parallel to the plane of the membrane; $R$ is the vertical distance above the membrane; and $\theta$, $\mu$, and $\varphi$ are the Euler angles that describe rotations about the peptide's geometric center. The average over the Boltzmann factor emphasizes the orientations of the lowest-interaction free energy. We use eq 11 to calculate the electrostatic component of the membrane binding of nonmyr-Src(2−19) (see Appendix I for details).

*Theoretical Model for Myristoylated Peptides*. In our model, we consider only the possibility that the myristate partitions into the membrane first, and not the possibility that the basic cluster partitions first. This approximation is reasonable because the partitioning due to the myristate is greater than the partitioning due to the basic cluster by 1−2 orders of magnitude (ref *15* and this report). As in the ball and string model, the myristate anchor restricts the basic cluster to a region of space above the membrane (Figure 1). We do not include an atomic representation of the myristate in our calculations, nor do we calculate $W_A$. We use the experimental result, $K_A$, to describe the hydrophobic contribution due to myristate insertion and solve the Poisson−Boltzmann equation to determine the electrostatic interaction between atomic models of the peptide and membrane. Thus, we calculate the membrane binding of myr-Src(2−19) using the expression

$$K \cong K_A\langle \exp[-W_B(x,y,R,\theta,\mu,\varphi)/kT]\rangle \tag{12}$$

where the broken brackets denote an average over orientations (see Appendix I for details). In contrast to our treatment of the nonmyristoylated peptide (where the peptide's orientations with respect to the membrane are unconstrained), we assume the N-terminal glycine of the myristoylated peptide is anchored outside the polar headgroup region of the membrane and the peptide is free to pivot about its N terminus (Figure 1). The orientations of the peptide with respect to the membrane are generated by rotating the peptide about the N-terminal glycine that is anchored 3 Å (i.e. one layer of water) from the membrane surface.

In the Gouy−Chapman limit for a point charge of valence $+Z$, $W_B$ in eq 12 is replaced by $eZ\phi(0)$:

$$K = K_A \exp[-eZ\phi(0)/kT] \tag{13}$$

where $\phi(0)$ is the surface potential of a membrane containing acidic phospholipids and $K_A$ is the measured adsorption of the molecule onto an electrically neutral membrane. This limiting form of eq 12 adequately describes the adsorption of small univalent molecules such as myristic acid (*16*), the fluorescent probe TNS, and spin-labeled probes (*46*) to negatively charged phospholipid vesicles, but cannot describe the adsorption of larger, multivalent peptides such as myr-Src(2−19), which have dimensions comparable to the Debye length.

*Molecular Models of Src(2−19) and Phospholipid Membranes*. Our model for the myristoylated peptide (Figure 1) is based on experimental studies of its structure and orientation with respect to the membrane. CD measurements (see Results) and direct structural electron paramagnetic resonance measurements (K. Victor and D. Cafiso, personal communication) suggest the peptide has a random coil conformation in solution and when bound to membranes. In agree-

ment with the experimental data, we built atomic models corresponding to residues 2−19 of Src (GSSKSKPKDPSQRRRSLE-$NH_2$) in extended form using the Biopolymer module of the Insight/Discover molecular modeling program (Insight-II, MSI). The extended conformation is often used to mimic a random coil conformation because all residues are solvated. This conformation is only one of many possible conformations the actual (random coil) peptide may assume. However, by sampling many different orientations of the peptide with respect to the membrane in the Poisson−Boltzmann calculations, we effectively describe the random coil state. To correspond to the peptides used in the binding measurements, we constructed models of nonmyristoylated peptides unblocked at the N terminus and models of both nonmyristoylated and myristoylated peptides blocked with an amide ($NH_2$) at the C terminus. To reduce atomic overlaps and to relax torsional and dihedral constraints, the models were energy minimized in the gas phase using the CVFF force field and neglecting electrostatic interactions. The minimizations, performed using the Insight/Discover program (INSIGHT-II, MSI), did not significantly alter the extended structure of the peptides.

Atomic models of negatively charged phosphatidylserine (PS) and zwitterionic phosphatidylcholine (PC) were built as described in Peitzsch et al. (*47*). Membrane bilayers are composed of hexagonally packed lipids in different proportions (1:0, 3:1, 2:1, 1:1, and 0:1 PC/PS) with the lipid species distributed uniformly. Each bilayer leaflet contains 192 or 360 lipids, with each lipid occupying an area of 68 $Å^2$ in the plane of the membrane (see Figure 1).

*Parameter Sets.* In the Poisson−Boltzmann calculations, the peptide and membrane are characterized by a set of atomic radii and partial charges (see Appendix I). The charge distribution within each phospholipid is taken from Charifson et al. (*48*), and van der Waals radii are used for the atoms. The charges and radii used for the peptide atoms are from the CHARMM22 parameter set (*49*). Previous work (*26*) has shown that the calculational results are insensitive to the particular parameter set employed.

## RESULTS

### *Experiments*

*Circular Dichroism and Monolayer Adsorption Measurements.* The crystal structure of c-Src was recently solved, revealing how intramolecular binding of the SH2 domain to a phosphorylated C-terminal tyrosine (tyrosine 527) inhibits kinase activity (*50*); the N terminus of the protein, which contains the two membrane-binding motifs, was not included in this structure. CD measurements (not shown) indicate that N-terminal Src peptides are in a random, extended conformation both in solution and when bound to small unilamellar vesicles (Figures 1 and 2). Nonmyr-Src(2−19) does not increase the surface area of a monolayer containing acidic phospholipids held at constant surface pressure, indicating the peptides do not penetrate the polar headgroup region of the monolayer (not shown). These observations have been confirmed and extended by direct electron paramagnetic resonance (EPR) measurements on spin-labeled myr-Src(2−16) peptides (K. Victor and D. Cafiso, personal communication); the peptide has an extended conformation, and its amino acid residues lie outside the envelope of the polar headgroup region. Our atomic models of the peptide are based on this structural information.

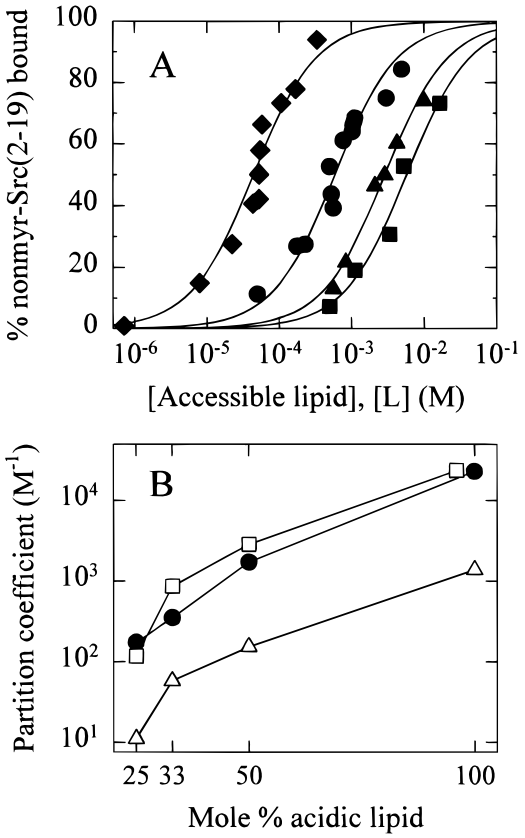


FIGURE 3: The membrane binding of nonmyristoylated peptides corresponding to residues 2−19 of Src (GSSKSKPKDPSQRRRSLE-$NH_2$) increases as the mole percent of acidic phospholipid in the membrane increases. (A) Partitioning of nonmyr-Src(2−19) onto large (100 nm diameter) unilamellar phospholipid vesicles (LUV). The results were obtained with a sucrose-loaded vesicle assay using LUV formed from 3:1 PC/PG (■), 2:1 PC/PG (▲), 1:1 PC/PG (●), and 0:1 PC/PG (◆) in 100 mM KCl buffered to pH 7.0 with 1 mM MOPS. Here, and in Figures 4A and 5, each plotted point is the average of at least two samples at that lipid concentration; the errors associated with the points are <10%. The curves are the least-squares fit of eq 5 to the data. (B) The molar partition coefficient determined experimentally from the data shown in panel A (●) and predicted from the theoretical model (△ and □) is plotted as a function of the mole percent of acidic lipid. Here, and in Figure 4, the experimental *K* values are uncertain by approximately 20%; see the text for uncertainties associated with the calculated *K* values. Here, and in Figure 4B, the open triangles are the predictions for *K* calculated by averaging over many orientations of the peptide with respect to the membrane (eq AI.3), and the open squares are approximate values for *K* calculated by considering only the orientation of maximum interaction.

*Partitioning of nonmyr-Src(2−19) onto Phospholipid Vesicles and the Effect of the Mole Percent of Acidic Lipid and Ionic Strength.* The nonmyr-Src(*2−19*) peptide contains six basic and two acidic residues and has a net charge of +5 at neutral pH (GSSKSKPKDPSQRRRSLE-$NH_2$). Figure 3A illustrates the partitioning of nonmyr-Src(2−19) onto phospholipid LUV containing 25, 33, 50, and 100 mole percent of acidic lipid in 100 mM KCl. The filled circles in Figure 3B are the values of *K* determined by fitting the data in Figure 3A with eq 5; increasing the mole percent of acidic lipid from 25 to 100% increases *K* 100-fold. This steep dependence of binding on the mole percent of acidic lipid is characteristic of multivalent basic peptides (*15*, *26*, *32*, *51*).

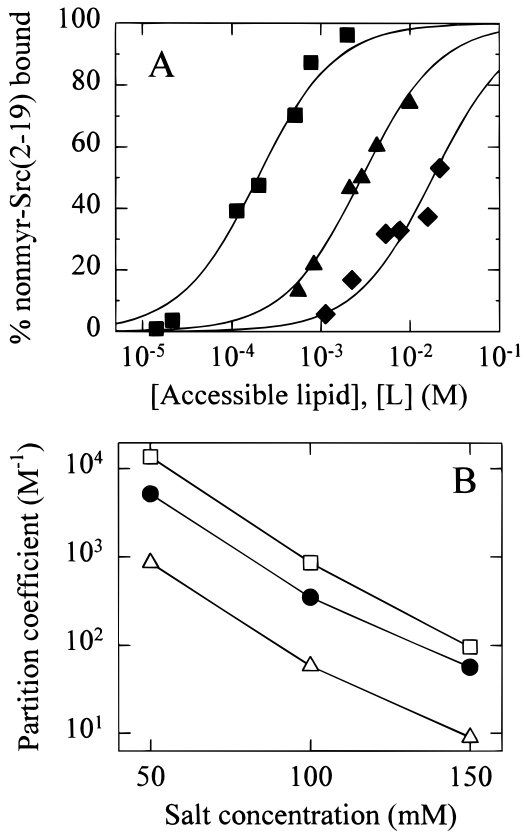


FIGURE 4: The membrane binding of nonmyristoylated peptides corresponding to residues 2−19 of Src (GSSKSKPKDPSQRRRSLE-$NH_2$) decreases as the salt concentration increases. (A) Binding of nonmyr-Src(2−19) to large unilamellar phospholipid vesicles. The results were obtained with a sucrose-loaded vesicle assay using LUV formed from 2:1 PC/PG in 50 mM (■), 100 mM (▲), and 150 mM (◆) KCl solutions. (B) The molar partition coefficient determined experimentally (see the binding data shown in panel A) (●) and predicted from the theoretical model (△ and □) is plotted as a function of monovalent salt concentration.

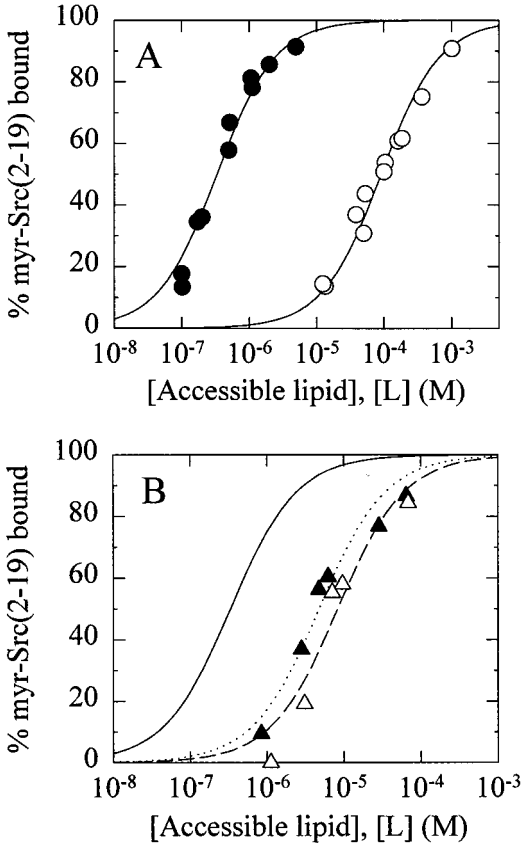


FIGURE 5: Membrane binding of myristoylated peptides corresponding to residues 2−19 of Src (GSSKSKPKDPSQRRRSLE-$NH_2$). The results were obtained with a sucrose-loaded vesicle assay using LUV formed from PC and PG in 100 mM KCl buffered to pH 7.0 with 1 mM MOPS. (A) Synergism of the N-terminal membrane binding motifs. Myr-Src(2−19) partitions onto neutral LUV formed from 1:0 PC/PG (○) with a $K$ of $1.1 \times 10^4 \pm 7.1 \times 10^2$ M$^{-1}$. Myr-Src(2−19) partitions 300-fold more strongly onto LUV formed from 2:1 PC/PG (●). The combination of myristate insertion and electrostatic attraction of basic residues to acidic lipids produces strong membrane binding of myr-Src(2−19) where $K = 3.0 \times 10^6 \pm 6.6 \times 10^5$ M$^{-1}$. (B) Phosphorylation causes desorption of Src peptides. Myr-Src(2−19) partitions onto LUV formed from 2:1 PC/PG with a $K$ of $3.0 \times 10^6$ M$^{-1}$ (solid curve). Myr-Src(2−19) phosphorylated by protein kinase C (△) or cAMP-dependent protein kinase (▲) partitions onto 2:1 PC/PG LUV with a $K$ of $1.2 \times 10^5 \pm 2.7 \times 10^4$ M$^{-1}$ or a $K$ of $2.1 \times 10^5 \pm 2.9 \times 10^4$ M$^{-1}$, respectively.

As discussed below, the increased binding is due to a nonspecific electrostatic effect. Nonmyr-Src(2−19) does not partition significantly onto electrically neutral PC vesicles (not shown), suggesting that nonelectrostatic interactions do not play a significant role in the association of the nonmyristoylated peptide with phospholipid membranes.

Figure 4A illustrates the partitioning of nonmyr-Src(2−19) onto 2:1 PC/PG LUV in 50, 100, and 150 mM KCl. The filled circles in Figure 4B are the values of $K$ determined by fitting the data in Figure 4A with eq 5; increasing the ionic strength from 50 to 150 mM KCl reduces $K$ 100-fold. At higher salt concentrations, the binding of nonmyr-Src(2−19) is too weak to measure accurately.

The experimental results shown in Figures 3 and 4 are consistent with our hypothesis that the binding of nonmyr-Src(2−19) is due mainly to a Coulombic attraction between the positively charged peptide and the negatively charged vesicles; $K$ increases as either the mole percent of acidic lipid increases or the ionic strength decreases. Similar effects have been observed with simple basic peptides (*26*) and the basic toxin charybdotoxin (*27*).

*Partitioning of Myr-Src(2−19) onto Electrically Neutral Phospholipid Vesicles.* Myr-Src(2−19) binds to electrically neutral PC LUV with a molar partition coefficient $K$ of $10^4$ M$^{-1}$ (or a unitary Gibbs free binding energy of 8 kcal/mol) (Figure 5A); the same value of $K$ has been reported for simple myristoylated peptides such as myr-glycine (*16*, *18*), myr-Src(2−12), and myr-Src(2−16) (*15*). Measurements of the membrane partitioning of fatty acids and acylated peptides reveal a linear increase in the binding energy as the number of carbon atoms in the acyl chains increases (*16*). The slope of 0.8 kcal/mol per $CH_2$ group is similar to that observed by Tanford (*52*) for the partitioning of the neutral forms of fatty acids into a bulk alkane phase from water. Our model (Figure 1) is consistent with these results: 8/0.8 (=10) $CH_2$ groups of myr-Src(2−19) partition into the

[3] This simplified picture ignores two contributions to the partitioning that approximately cancel. (a) The $CH_3$ group at the tail of the myristate contributes an additional 1 kcal/mol to the partitioning due to its larger water-accessible surface area (*52*). (b) The myristate, which has a cross-sectional area $\Delta A$ of 25 Å$^2$, must do work to insert into the monolayer ($\pi\Delta A \approx 1$ kcal/mol or $5 \times 10^3$ J/mol) where $\pi \approx 0.04-0.05$ kcal mol$^{-1}$ Å$^{-2}$ or 30−35 mN/m (*34*, *53*).

hydrocarbon interior of the membrane, 4 $CH_2$ groups traverse the polar headgroup region, and the N-terminal glycine is located immediately outside the polar headgroup region.[3] Measurements with spin-labeled peptides provide strong independent support for the structure shown in Figure 1 (K. Victor and D. Cafiso, personal communication).

*Synergism between the Myristate and Basic Cluster Results in Strong Partitioning of Myr-Src(2−19) onto Phospholipid Vesicles Containing Acidic Phospholipids*. The myr-Src-(2−19) peptide (myristate-GSSKSKPKDPSQRRRSLE-$NH_2$), which has a net charge of +4 at neutral pH, binds 300-fold more strongly to 2:1 PC/PG LUV than to electrically neutral PC LUV (Figure 5A). A similar effect was reported for myr-Src(2−16), which has a net charge of +5, and for the intact c-Src protein; membrane binding increased 1000-fold upon incorporation of 33% acidic phospholipid into PC vesicles (*11*, *15*). Myr-Src(2−19) associates strongly with 2:1 PC/PG vesicles by a combination of hydrophobic insertion of myristate and electrostatic attraction between basic residues and acidic phospholipids. The synergism between the two membrane binding motifs is illustrated by noting that, for a lipid concentration of $10^{-5}$ M, electrostatic interactions alone bind only 1% of the peptide (triangles, Figure 3A), hydrophobic interactions alone bind only 10% of the peptide (open circles, Figure 5A), but the two interactions together bind >90% of the peptide (solid circles, Figure 5A).

*Effect of Phosphorylation on the Partitioning of Myr-Src-(2−19) onto Phospholipid Vesicles*. The N-terminal region of Src contains phosphorylation sites at serine 12 and serine 17. Phosphorylation of either site reduces the net peptide charge from +4 to +2 (Figure 2). Figure 5B shows that *K* for 2:1 PC/PG LUV decreases 15−25-fold following phosphorylation of myr-Src(2−19) by either PKC or PKA. As expected, phosphorylation does not affect the partitioning of myr-Src(2−19) onto electrically neutral PC LUV (not shown). Experiments with simple basic peptides ($Lys_7$, $Lys_5$, and $Lys_3$) showed a similar (30-fold) decrease in membrane binding as the number of lysine residues (and thus net charge) in the peptides decreases by 2 (*26*).

*Effect of Phosphorylation on Membrane Localization of Src in Vivo*. These experiments were designed to assess whether phosphorylation of serine residues within the N-terminal region of Src could regulate Src binding to biological membranes. The sequences encoding the first 20 amino acids of Src were fused in-frame to a heterologous soluble carrier protein, $\beta$-galactosidase ($\beta$Gal), and the chimeric protein was expressed in COS-1 cells. Subcellular fractionation revealed that Src20$\beta$Gal was predominantly localized to the particulate (membrane) fraction. In contrast, native $\beta$Gal was almost totally confined to the cytosolic fraction. Radiochemical labeling was performed to assess the phosphorylation state of the chimeric protein. As illustrated in Figure 6, attachment of the Src20 sequence to $\beta$Gal resulted in phosphorylation of the fusion protein. The major site of phosphorylation was most likely serine 17, because $^{32}P$ incorporation was much lower in the S17A Src20$\beta$Gal mutant than in Src20$\beta$Gal. This is in agreement with previous studies where $pp60^{v-src}$ protein was shown to be constitutively phosphorylated on serine 17 (*54*). We were not able to observe significant phosphorylation of serine 12, even when the cells were stimulated with phorbol myristate acetate (PMA) to activate PKC. We then examined the effect of phosphorylation on Src$\beta$Gal localization. COS-1 cells expressing Src$\beta$Gal were labeled with $^{32}P$-orthophosphate, lysed, and fractionated into membrane and cytosolic fractions. Samples were first analyzed for total Src20$\beta$Gal protein by immunoprecipitation and Western blotting using anti-$\beta$Gal antibody. The blots were then bleached and reanalyzed by phosphorimaging for the presence of $^{32}P$-labeled Src20$\beta$Gal. In four experiments, 15.3% (±3%) of the total Src20$\beta$Gal protein was located in the S-100 cytosolic fraction. However, approximately 1.5-fold more phosphorylated Src20$\beta$Gal protein (22.6 ± 6%) was found in the S-100 fraction when $^{32}P$-labeled protein was analyzed. An identical 1.5-fold shift was observed for the S12A Src20$\beta$Gal protein; this protein is phosphorylated to the same extent as wild-type Src20$\beta$Gal. Thus, there is a small but detectable shift of some of the phosphorylated Src20$\beta$Gal protein from the membrane to the cytosol upon phosphorylation.

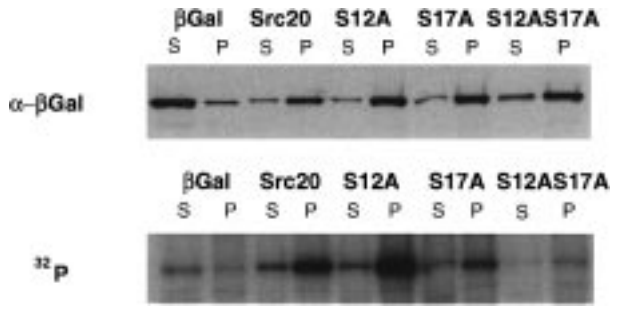


FIGURE 6: Subcellular distribution of wild-type and mutant Src20$\beta$Gal constructs. COS cells were transfected with plasmids containing the indicated Src sequence fused to $\beta$Gal. Cells were radiolabeled with $^{32}P$-orthophosphate and fractionated into cytosolic (S) and membrane (P) fractions. The total amount of $\beta$Gal fusion protein in each fraction was determined by immunoprecipitation and Western blotting with anti-$\beta$Gal antibody (upper panel). The blots were bleached and reanalyzed by phosphorimaging (lower panel) to quantitate the amount of $^{32}P$-labeled Src$\beta$Gal protein.

### *Theoretical Model*

*Electrostatic Free Energy of Interaction*. Figure 7 plots the electrostatic free energy of interaction ($W_B$, eq AI.3) between nonmyr-Src(2−19) and a 2:1 PC/PS bilayer in a 100 mM monovalent salt solution as a function of the distance, *R*, between the van der Waals surfaces of the peptide and bilayer. The peptide is oriented to optimize the electrostatic interaction; in Figure 2A, the membrane would be below and parallel to the peptide, as illustrated in Figure 1 for the myristoylated peptide. The orientation of maximum interaction was estimated by visually inspecting the peptide's electrostatic potential profile with the program GRASP (Figure 2A) (*55*).

As the positively charged peptide approaches the membrane, it experiences a Coulombic attraction to the negatively charged bilayer. This long-range attraction ($R \geq 3$ Å; Figure 7) gives rise to the binding we measure experimentally. At shorter distances ($R < 3$ Å), however, portions of the peptide and lipid headgroups are no longer accessible to water and can be thought of as being transferred from a high-dielectric region ($\epsilon_r = 80$) to a low-dielectric region ($\epsilon_r = 2$). This transfer of charge from high- to low-dielectric regions is energetically unfavorable and gives rise to a Born repulsion (or desolvation force) that dominates the electrostatic attrac-

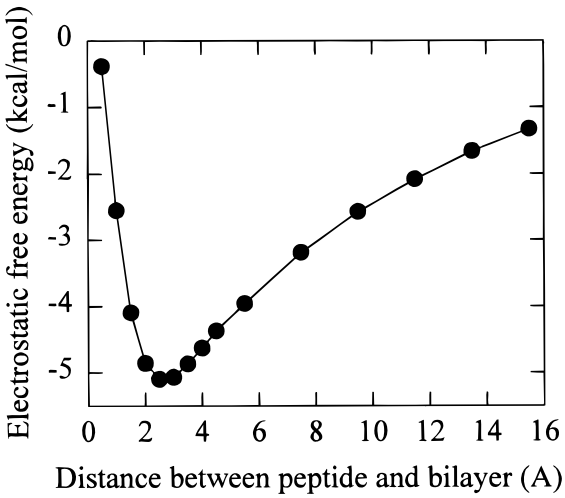


FIGURE 7: Electrostatic free energy curve obtained from the calculations. The curve depicts the electrostatic free energy of interaction between nonmyristoylated Src(2−19) and a 2:1 PC/PS bilayer in 100 mM monovalent salt as a function of the distance, *R*, between the molecules' van der Waals surfaces. The peptide is oriented with respect to the membrane surface to optimize the electrostatic interaction; in Figure 2A, the membrane would be below and parallel to the peptide. The balance between the long-range Coulombic attraction and short-range Born repulsion results in the free energy minimum at $R \sim 3$ Å.

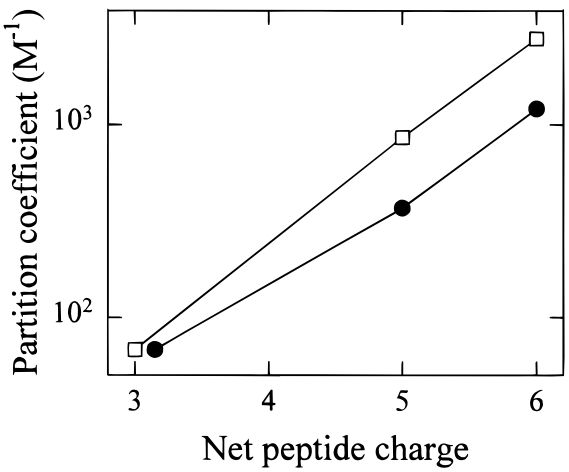


FIGURE 8: The membrane binding of nonmyristoylated peptides corresponding to the N terminus of Src increases as the net charge of the peptide increases. The filled circles are the molar partition coefficients determined from experimental measurements of the binding of nonmyr-Src(2−12) (net charge of +3), nonmyr-Src(2−19) (net charge of +5), and nonmyr-Src(2−16) (net charge of +6) to 2:1 PC/PS LUV in 100 mM KCl based on data from this paper and from Buser et al. (*15*). The open squares are approximate values for *K* calculated by considering only the orientation of maximum interaction.

tion at short distances (*26*, *56*, *57*). The balance between the short-range repulsive and long-range attractive interactions results in the energy minimum at $R \sim 3$ Å. The model describes well the long-range attractive interaction ($R \geq 3$ Å), as illustrated by the theoretical predictions discussed below.

*Electrostatic Interaction and Membrane Partitioning of Nonmyristoylated Peptides.* We calculated energy curves, like the one depicted in Figure 7, for each of 20 randomly sampled orientations of nonmyr-Src(2−19) with respect to the membrane (see Appendix II). The Boltzmann factors of the interaction energies from each curve were averaged at each *R* ($0 < R \leq 20$ Å) to calculate the electrostatic component of *K* in eq AI.3 (Appendix I).

The open triangles in Figure 3B show the theoretical predictions for *K* as a function of the mole percent of acidic lipid; the model predicts the partitioning of nonmyr-Src(2−19) onto PC/PS bilayers in a 100 mM salt solution increases about 100-fold when the mole percent of acidic lipid increases from 25 to 100%. This agrees well with the 100-fold increase observed experimentally (Figure 3B, filled circles). Adding acidic lipid to the bilayer increases the magnitude of the negative surface potential adjacent to the membrane, deepening the minimum of the free energy curve (Figure 7), and producing a stronger electrostatic attraction of the basic residues to the membrane surface. The model also predicts nonmyr-Src(2−19) does not interact significantly with an electrically neutral PC bilayer (calculations not shown), as observed experimentally.

The open triangles in Figure 4B show the theoretical predictions for *K* as a function of monovalent salt concentration; the partitioning of nonmyr-Src(2−19) onto 2:1 PC/PS bilayers decreases about 100-fold when the ionic strength increases from 50 to 150 mM. This agrees well with the 100-fold decrease observed experimentally (Figure 4B, filled circles). Increasing the ionic strength of the solution decreases the Debye length and the magnitude of the membrane surface potential, decreasing the depth and width of the free energy curve (Figure 7).

The open squares in Figure 8 show the theoretical predictions for an approximate partition coefficient (see below) as a function of net peptide charge; increasing the net charge on the peptide from +3 to +6 should increase its partitioning onto 2:1 PC/PS bilayers in a 100 mM salt solution 40-fold. We observe a 20-fold increase experimentally (Figure 8, filled circles). Increasing the net charge of the peptide increases the long-range Coulombic attraction between the peptide and the negatively charged membrane.

Approximate values for *K* were calculated by considering only the orientation of maximum interaction (Figure 7); at each *R* in the integral of eq AI.3, only the Boltzmann factor of the interaction energy for this single orientation was included. The agreement between the approximate *K* values and the experimental values is fortuitous. These estimates predict the relative binding trends well (open squares in Figures 3B, 4B, and 8). Similar results have been reported for simple basic peptides (*26*) and toxins (*27*). The success of the approximate values in describing the relative binding is significant because averaging over many orientations in the Gibbs surface excess calculations is computationally intensive.

*Combining Electrostatic and Hydrophobic Interactions for Membrane Partitioning of Myristoylated Peptides.* We used eq 12 to calculate the partitioning of myr-Src(2−19) onto phospholipid bilayers; 50 different orientations of the peptide were included in the calculations (Appendix II). The model predicts myr-Src(2−19) binds 100-fold more strongly to 2:1 PC/PS bilayers than to neutral PC bilayers, which agrees qualitatively with the 300-fold increase observed (line 1 of Table 1). In contrast, the model based on Gouy−Chapman theory (eq 13) predicts a 10000-fold increase. Our model predicts myr-Src(2−12) (myr-GSSKSKPKDPS-$NH_2$, net charge of +2) binds 10-fold less strongly than myr-Src(2−

Table 1: Relative Membrane Partitioning of Myristoylated Src Peptides[a]

| relative membrane association | fold change in $K$ | |
|---|---|---|
| | experiment | theory |
| [myr-Src(2−19), 2:1 PC/PS]/ [myr-Src(2−19), PC] | 300 | 100 |
| [myr-Src(2−12), 2:1 PC/PS]/ [myr-Src(2−19), 2:1 PC/PS] | $^1/_{10}$ | $^1/_{10}$ |
| [pS12, 2:1 PC/PS]/ [wt, 2:1 PC/PS] | $^1/_{25}$ | $^1/_5$ |
| [pS17, 2:1 PC/PS]/ [wt, 2:1 PC/PS] | $^1/_{15}$ | $^1/_3$ |

[a] Myr-Src(2−19), myristate-GSSKSKPKDPSQRRRSLE-$NH_2$, net charge of +4; myr-Src(2−12), myristate-GSSKSKPKDPS-$NH_2$, net charge of +2; pS12, myr-Src(2−19) phosphorylated at Ser12, net charge of +2; pS17, myr-Src(2−19) phosphorylated at Ser17, net charge of +2; 2:1 PC/PS, 2:1 PC/PS LUVs in a 100 mM monovalent salt solution; PC, PC LUVs in a 100 mM monovalent salt solution.

19) to 2:1 PC/PS membranes, which agrees with the 10-fold decrease observed experimentally (line 2 of Table 1).

*Phosphorylation*. Phosphorylation of either serine 12 or serine 17 in myr-Src(2−19) reduces the net charge of the peptide from +4 to +2; the consequent reduction in the electrostatic potential adjacent to the peptide (Figure 2) reduces the electrostatic attraction between the basic peptide and acidic lipids. The model predicts phosphorylation of myr-Src(2−19) reduces its interaction with a 2:1 PC/PS bilayer about 5-fold, which agrees qualitatively with the 15−25-fold reduction observed (lines 3 and 4 of Table 1). Our results indicate that the decreased electrostatic attraction of myr-Src(2−19) to acidic phospholipid bilayers can account for the effect of phosphorylation on membrane association.

## DISCUSSION

Previous work showed that both hydrophobic and electrostatic interactions are required to anchor Src to membranes, and that peptides corresponding to the N terminus of Src bind to phospholipid membranes in a manner similar to that of the intact protein (*11*, *15*). We have developed a theoretical model (*26*, *27*) that describes the role of electrostatic interactions in the association of Src(2−19) with phospholipid membranes. Using atomic models, we calculated the electrostatic component of the membrane binding of nonmyr-Src(2−19) and myr-Src(2−19). We augmented our earlier experimental studies (*15*) by analyzing the membrane binding of nonmyr-Src(2−19) and the effect of phosphorylation of serine 12 and serine 17 on binding of either myr-Src(2−19) to phospholipid vesicles or Src chimeras to biological membranes. The theoretical predictions agree qualitatively with the experiments. Our measurements (*11*, *15*) and theoretical results are consistent with the hypotheses that Src's N-terminal cluster of basic residues interacts electrostatically with acidic phospholipids and that phosphorylation weakens this interaction.

We built atomic models of Src(2−19) based on information from CD, EPR, and monolayer measurements, and docked the peptide in a continuum aqueous phase adjacent to atomic models of phospholipid membranes. Using the nonlinear Poisson−Boltzmann equation and the concept of the Gibbs surface excess, we calculated the electrostatic component of the binding of nonmyr-Src(2−19) to PC/PS bilayers. The model predicts how the association of nonmyr-Src(2−19) with phospholipid bilayers increases upon (a) increasing the mole percent of acidic lipid in the bilayer (Figure 3B), (b) decreasing the ionic strength of the solution (Figure 4B), or (c) increasing the net charge of the peptide (Figure 8); similar results were reported previously for small basic peptides (*26*) and toxins (*27*). We extended the theoretical methodology to describe the membrane binding of myristoylated peptides, and the calculations predict how the binding of myr-Src(2−19) increases upon incorporation of acidic phospholipids into PC bilayers (Table 1). In contrast to simpler models that depict myr-Src(2−19) as two dimensionless points, our model provides a more realistic, molecular picture of how the apparent cooperativity between the myristate and basic cluster arises. Our theoretical approach should be applicable to other lipid-modified proteins with basic clusters that interact with acidic phospholipids, e.g. K-Ras 4B (*21*, *22*) and HIV-1 matrix protein (*58*−*60*).

Nevertheless, the model has important limitations. Calculations based on electrostatics alone consistently underestimate the measured partition coefficients of simple basic peptides (*26*), basic toxins (*27*), and Src(2−19) (Figures 3B, 4B, and 8 and Table 1) by about 1 order of magnitude; this implies the model may overestimate the repulsive short-range electrostatic interactions, ignore some short-range attractive interactions, or both. The peptide and bilayer in our model are static and do not change structure upon association. The charged and polar groups of these molecules may rearrange themselves to maximize the electrostatic attraction and/or minimize the Born repulsion. Ben-Tal et al. (*27*) recently showed that incorporating attractive nonpolar interactions between the peptide and membrane into the model (estimated as the product of a surface tension coefficient and the reduction in water-accessible surface area of the peptide and bilayer upon association; see Appendix III) can reduce the discrepancy between the theoretical predictions and experimental results. Including nonpolar contributions in the calculation of $K$ for nonmyr-Src(2−19) overestimates the measured partition coefficient 5-fold (see Appendix III). Although experimental measurements (e.g. this report and refs *26* and *61*) indicate that peptides such as nonmyr-Src(2−19) do not penetrate the polar headgroup region, it is not known to what extent desolvation occurs upon association. Further theoretical (*62*, *63*) and experimental (*64*) work is required to obtain a more accurate description of short-range protein/membrane interactions.

The presence of phosphorylation sites within Src's N-terminal basic cluster suggests a potential mechanism for reversing its association with membranes; phosphorylation weakens the electrostatic attraction of Src to acidic phospholipids. Our results and calculations indicate that phosphorylation of either serine 12 or serine 17 decreases the partitioning of myr-Src(2−19) onto 2:1 PC/PG vesicles (Table 1). Chimeric constructs of Src's N terminus and soluble carrier proteins are singly phosphorylated in COS-1 cells: although the chimeras were constitutively phosphorylated at serine 17, we were unable to detect significant phosphorylation of serine 12. The partition coefficient of myr-Src(2−19) phosphorylated at serine 17 is $10^5$ $M^{-1}$ under physiological conditions (Figure 5B). Previous studies showed the hydrophobic anchoring is about 10-fold weaker

for the Src protein than for peptides based on the N terminus of Src (*11*, *15*); thus, we expect the partition coefficient of the monophosphorylated protein to be $\sim 10^4$ $M^{-1}$. For a spherical cell with a radius of 10 $\mu$m, the accessible lipid concentration is $\sim 10^{-3}$ M, so most of the monophosphorylated protein should be membrane-bound. Our in vivo studies with Src chimeras are consistent with this expectation (Figure 6). Only if both serines are phosphorylated would we expect Src to desorb significantly from a biological membrane.

The effect of serine 12 and serine 17 phosphorylation on Src protein function is unknown. Mutation of serine 12 and/or serine 17 in v-Src or activated c-Src prevents phosphorylation at these sites but has no effect on cellular transformation or kinase activity (*54*, *65*). Other investigators have reported increased kinase activity when c-Src is phosphorylated in its N-terminal region; this may be related to enhanced dephosphorylation of the negative regulatory tyrosine 527 via some unknown intermediate event (*66*, *67*). Mutation of serine 12 to alanine reduces the responsiveness to $\beta$-adrenergic agonists in cells overexpressing c-Src (*68*) and leads to increased association between PKC-$\delta$ and c-Src (*69*). Correlations between c-Src localization and N-terminal phosphorylation have been observed in specific cell types. For example, treatment of 3T3 fibroblasts with PDGF results in translocation of c-Src from the plasma membrane to the cytosol, concomitant with an increase in N-terminal phosphorylation by PKA, presumably at serine 17 (*29*). We, however, have been unable to detect c-Src translocation in NIH 3T3 cells treated with PDGF (C. T. Sigal and M. D. Resh, unpublished data). Finally, growth factor (PDGF or EGF) or agonist (thrombin) stimulation of cells has been reported to induce c-Src translocation to the cytoskeleton (*30*, *66*). These agents have been shown to induce phosphorylation of c-Src at serine 12 (*70*, *71*). Thus, phosphorylation within Src's N terminus may affect the function of Src by modulating its interactions with other proteins and/or its cellular localization.

## APPENDIX I

*Theoretical Model.* Our model (*24*, *25*, *72*) depicts the peptide and membrane in atomic detail and water as a structureless medium (Figure 1). The univalent ions (e.g. $K^+$ and $Cl^-$) are dimensionless points, treated in the mean-field approximation. The theoretical methodology is described in detail elsewhere (*26*, *27*). Here we give a brief overview, focusing on details that are unique to the Src(2−19) system.

We assign to each atom of the peptide and bilayer a radius and a partial charge at its nucleus and then map the peptide/membrane model onto a three-dimensional lattice of points, each of which represents a small region of the peptide, membrane, or solvent (*25*). Smooth molecular surfaces for the peptide and membrane are generated by rolling a spherical probe with the radius of a water molecule (1.4 Å) over the surfaces defined by the van der Waals radii of the constituent atoms; the point of contact between the probe and the van der Waals surface defines the molecular surface. We assign a low dielectric constant of 2 to lattice points that lie within the molecular surfaces of the peptide and the membrane and a high dielectric constant of 80 to lattice points outside the molecular surfaces; the latter region represents the aqueous phase. Salt ions are excluded from a region that extends 2 Å (the radius of a $Na^+$ ion) beyond the van der Waals surfaces of the peptide and membrane (see Figure 3 in ref *26*). We calculate the electrostatic potential and the mean distribution of the monovalent salt ions at each lattice point by solving the nonlinear Poisson−Boltzmann equation numerically (ref *26* and references therein). A sequence of focusing runs of increasing resolution is employed to calculate the potentials (see Appendix III). In the initial calculation, the peptide fills approximately 6% of the lattice and the potential values at the boundary points of the lattice are approximately 0. This procedure ensures that the system is electroneutral. The solutions of the Poisson−Boltzmann equation are used to calculate the total electrostatic free energy of the system (*73*). The electrostatic free energy of interaction, $W_B$, is the difference between the electrostatic free energy when the peptide associates with the membrane ($W^{p+m}$) and the electrostatic free energy when the peptide and membrane are an infinite distance apart ($W^p + W^m$):

$$W_B(x,y,R,\theta,\mu,\varphi) = W_B^{p+m}(x,y,R,\theta,\mu,\varphi) - [W_B^p(x,y,R,\theta,\mu,\varphi) + W_B^m(x,y,R,\theta,\mu,\varphi)] \quad \text{(AI.1)}$$

The coordinates $x$, $y$, $R$, $\theta$, $\mu$, and $\varphi$ locate the peptide with respect to the membrane. $x$ and $y$ are translations in the plane of the membrane; $R$ is the vertical distance above the membrane; and $\theta$, $\mu$, and $\varphi$ are the Euler angles that describe rigid body rotations of the peptide. We use a single conformation for both the peptide and the membrane and, thus, do not account for the motion due to internal degrees of freedom.

We average over the different orientations of the peptide with respect to the membrane in the Gibbs surface excess calculations in order to approximate a complete ensemble of different configurations. The peptide concentration a distance $R$ from the membrane depends on the bulk peptide concentration and the average of the exponent of the free energy change, $W_B$, that occurs when the peptide moves from the bulk solution to $R$ (*26*, *74*):

$$[P(R)] = [P(\infty)]\langle \exp[-W_B(x,y,R,\theta,\mu,\varphi)/kT]\rangle \quad \text{(AI.2)}$$

Note that this formulation assumes the association is purely electrostatic. Equation AI.2 is the six-dimensional equivalent of eq 7. For each orientation, the interaction free energy between the peptide and membrane, $W_B$, is calculated at each $R$. Combining eqs 3, 8, 9, and AI.2 gives eq 11. We restrict the integral to 0 Å $\leq R \leq$ 20 Å, for which the integrand is dominated by the exponent. Equation 11 can then be approximated as follows:

$$K = A_L N \int_0^{20} dR\, \langle \exp[-W_B(x,y,R,\theta,\mu,\varphi)/kT] - 1\rangle \quad \text{(AI.3)}$$

$$\cong A_L N \int_0^{20} dR\, \langle \exp[-W_B(x,y,R,\theta,\mu,\varphi)/kT]\rangle$$

Equation AI.3 forms the basis of our calculations; it allows us to make theoretical predictions that can be compared with experimental measurements.

Our objective in these studies is to calculate changes in $K$ as a function of the mole percent of acidic lipid in the membrane, the ionic strength of the solution, and the net

charge on the peptide (including effects of phosphorylation). These changes are dominated by $W_B$. For a more general treatment, aimed at calculating the absolute value of $K$, the interaction energy can include additional terms that may contribute to the membrane binding: for example, $W_{np}$ for nonpolar contributions (see ref *27* and Appendix III) and $W_A$ for the hydrophobic insertion of myristate.

The binding of myr-Src(2−19) should, in principle, be calculated using eq AI.3 with $W_B$ replaced by $W_B + W_A$, where $W_A$ is a theoretical description of the interaction of myristate with the membrane. We did not include an atomic representation or a theoretical treatment of the myristate in our model. Including an explicit representation of the myristate would greatly increase the number of possible conformations of the peptide and, hence, the computational expense. The approximate model for the membrane binding of myr-Src(2−19) (eq 12) assumes the N-terminal glycine is located 3 Å (one layer of water) from the membrane surface. Since the interaction due to myristate insertion is stronger and of shorter range than the electrostatic interaction, we make the simplifying assumption that it is equal to the experimentally determined value, $K_A$, at $R = 3$ Å. By considering different orientations of the peptide rotated about the N-terminal glycine that is anchored 3 Å outside the polar headgroup region, our molecular model simulates the environment (i.e. the enhanced lipid concentration) experienced by the basic cluster after the myristate is inserted. In the ball and string model of eq 1, the coupling between the two binding sites appears explicitly as $2/(3r)$. In contrast, a coupling term cannot be factored out of our theoretical model (eq 12) for the partition coefficient of myr-Src(2−19); it is implicit in the construction of the model.

As described in the Results and Discussion, our theoretical model for the partitioning of Src peptides describes well the relative binding, but not the absolute partition coefficients. Among the conditions examined here (mole percent of acidic lipid, ionic strength, and net peptide charge), the differences in partitioning are driven by the long-range Coulombic attraction; contributions that are neglected or inadequately represented (e.g. nonpolar, short-range electrostatic, and entropic) are expected to be similar for the different experimental conditions. So upon the relative binding being calculated (by taking the ratio of the calculated molar partition coefficients), these contributions largely cancel, resulting in an accurate description of the relative electrostatic effects on binding.

## APPENDIX II

*Efficient Sampling Procedure for Generating Peptide Orientations*. The orientation of the peptide with respect to the fixed membrane is defined by three Cartesian coordinates ($x$, $y$, and $R$) and three Eulerian angles of rotation ($\theta$, $\mu$, and $\varphi$). The rotations are applied about the peptide's geometric center (nonmyristoylated peptides) or about the peptide's N terminus (myristoylated peptides). We developed an efficient algorithm for generating orientations of Src(2−19) with respect to the membrane by randomly choosing values from a uniform distribution for the three Euler angles ($\theta \in [0-\pi]$; $\mu$ and $\psi \in [0-2\pi]$) and the two translations within the membrane plane ($x$ and $y \in [-8$ to 8 Å$]$). The range of 16 Å for the $x$ and $y$ translations was chosen to correspond with

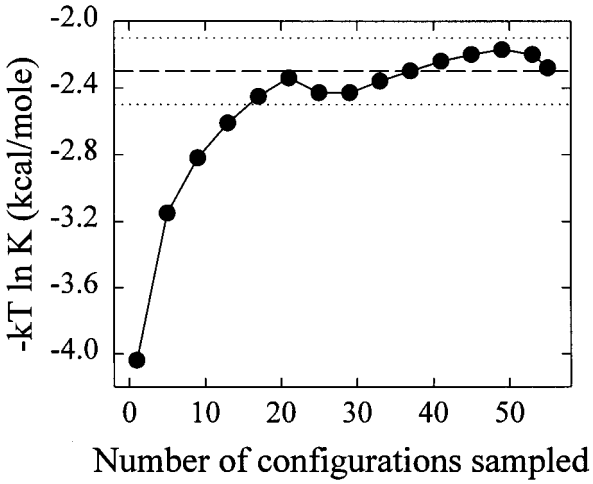


FIGURE 9: Calculated partition coefficient for nonmyr-Src(2−19) interacting with a 2:1 PC/PS bilayer in a 100 mM salt solution versus the number of configurations sampled. Convergence is achieved after 20 peptide orientations are included in eq AI.3. The dashed line is the bootstrap mean, and the dotted lines represent the standard deviation about this mean. See Appendix II for details.

the average distance between the acidic lipids distributed evenly in the model membranes.

*Convergence with Respect to the Number of Orientations.* Figure 9 shows the convergence of the calculated partition coefficient as a function of the number of orientations averaged over in eq AI.3. The partition coefficient is converged after 20 orientations are included in the calculation; the difference is insignificant when 55 orientations ($K = 47$ M$^{-1}$), rather than 20 ($K = 52$ M$^{-1}$), are included. We further assessed the convergence using Efron's bootstrap procedure (*75*), which determines how accurately a limited sample of data (e.g. energy curves for 55 orientations) represents the whole array of possible data (i.e. energy curves for all possible orientations). Our sample of data consists of 55 energy curves, one for each orientation of the peptide with respect to the membrane. A "new" sample of data is approximated by choosing randomly (with replacement) 55 energy curves from the original sample. We generated 1000 different sets of 55 energy curves, calculated a partition coefficient for each, and used these partition coefficients to determine the bootstrap mean and standard deviation (dashed and dotted lines in Figure 9). The bootstrap mean partition coefficient and standard deviation do not differ significantly from the value of the partition coefficient determined with 20 orientations; this indicates sufficient convergence with respect to the number of orientations sampled.

*Convergence of $W_B$.* We calculate the electrostatic free energies in eq AI.1 by solving the Poisson−Boltzmann equation numerically (*26*). For most calculations, a grid size of $113^3$ was used with a sequence of focusing runs (0.25, 0.5, and 1.0 grid/Å). Results obtained using a grid size of $113^3$ differed by less than 0.2 kcal/mol between the 0.5 and 1.0 grid/Å scales at $R \geq 3$ Å. Comparable calculations performed on larger grids ($177^3$ or $193^3$) to a finer resolution (2 grid/Å) differed from the lower-resolution calculations by less than 0.2 kcal/mol at $R \geq 3$ Å. Calculations for the partition coefficient of nonmyr-Src(2−19) for a 2:1 PC/PS membrane in 100 mM salt were performed on a grid of $177^3$ to a resolution of 2 grid/Å; the result obtained with the high-resolution calculations (68 M$^{-1}$) differed insignificantly from

Table 2: Effect of Including Nonpolar Contributions in the Calculation of the Molar Partition Coefficient for Myr-Src(2−19) Binding to 2:1 PC/PS Membrane in 100 mM Salt

| condition | $K$ ($M^{-1}$) |
|---|---|
| experiment | 300 |
| high-resolution calculation with electrostatics | 70 |
| high-resolution calculation with electrostatics and nonpolar | 1600 |
| low-resolution calculation with electrostatics | 50 |
| low-resolution calculation with electrostatics and nonpolar | 100 |

the lower-resolution calculation (52 $M^{-1}$). Combining uncertainties arising from the calculation of the interaction energies and from the finite sampling of orientations, we estimate the binding constants are precise to within 0.5 kcal/mol, which corresponds to a 2-fold uncertainty in $K$ (see ref *26* for a detailed discussion of convergence issues).

## APPENDIX III

*Nonpolar Contributions to the Partitioning of Nonmyristoylated Src(2−19).* Ben-Tal et al. (*27*) included nonpolar contributions, $W_{np}(x,y,R,\theta,\mu,\varphi)$, in eq AI.3; $W_B$ is replaced by $W_B + W_{np}$. $W_{np}$ is calculated by assuming it is proportional to the change in water-accessible surface area of the peptide and membrane as they approach each other:

$$W_{np}(x,y,R,\theta,\mu,\varphi) = \gamma[A(x,y,R,\theta,\mu,\varphi) - A^{max}] \quad \text{(AIII.1)}$$

where $\gamma = 28$ cal $mol^{-1}$ $Å^{-2}$ is a surface tension coefficient derived from the partitioning of alkanes between water and liquid alkanes (*76*), $A$ is the water-accessible surface area of the peptide−membrane complex when the peptide has coordinates $x$, $y$, $R$, $\theta$, $\mu$, and $\varphi$, and $A^{max}$ is the water-accessible surface area when the peptide and membrane are infinitely far apart. The water-accessible surface area is calculated using a modified Shrake and Rupley algorithm (*77*). When nonpolar contributions (eq AIII.1) are included, the calculated molar partition coefficient for charybdotoxin binding to a 2:1 PC/PS membrane in 100 mM salt agrees more closely with the measured value (*27*).

Table 2 compares measured and calculated $K$ values for nonmyr-Src(2−19) binding to a 2:1 PC/PS membrane in 100 mM salt. The calculations were performed with and without nonpolar contributions under two conditions: "high" corresponds to Poisson−Boltzmann calculations performed on a $177^3$ grid to 2 grid/Å resolution, and "low" corresponds to Poisson−Boltzmann calculations performed on a $113^3$ grid to 1 grid/Å resolution. The theoretical prediction for $K$ considering only the electrostatic component underestimates the measured value by a factor of 4 (lines 1 and 2 of Table 2); including nonpolar contributions overestimates it by a factor of 5 (lines 1 and 3 of Table 2).

The calculation of $K$ including only the electrostatic component of the interaction energy is relatively insensitive to the resolution of the Poisson−Boltzmann calculation (lines 2 and 4 of Table 2). Although $W_{np}$ is independent of the resolution of the Poisson−Boltzmann calculations, the calculation of $K$ including nonpolar contributions is highly sensitive to the resolution (lines 3 and 5 of Table 2). Figure 10 illustrates how the free energy curve for the orientation of maximal interaction (Figure 7) changes when nonpolar contributions are included. The convergence of $W_B$ at $R \geq 3$ Å is good at both high and low resolutions (see Appendix II), but deteriorates at $R < 3$ Å; for example, $W_B$ differs between the low- and high-resolution calculations by 2.5 kcal/mol at $R = 1.5$ Å but only 0.1 kcal/mol at $R = 3.5$ Å. When the peptide is close to the membrane ($R < 3$ Å), $W_B$ is dominated by the Born repulsion (Figure 10, circles). The interaction energies in this region receive less weight in the Boltzmann average of eq AI.3 than the more negative interaction energies at $R \geq 3$ Å; this accounts for the robustness of the calculated electrostatic binding with respect to resolution. $W_{np}$ is significant at $R < 3$ Å (Figure 10, squares); hence, the sum $W_B + W_{np}$ is very sensitive to the value of $W_B$ in this region (Figure 10, triangles), which explains the discrepancy between the low- and high-resolution cases (lines 3 and 5 of Table 2). Because of the problems associated with convergence of $W_B$ in the region $R < 3$ Å, we can make only the qualitative statement that inclusion of nonpolar contributions increases the calculated molar partition coefficients (Table 2).

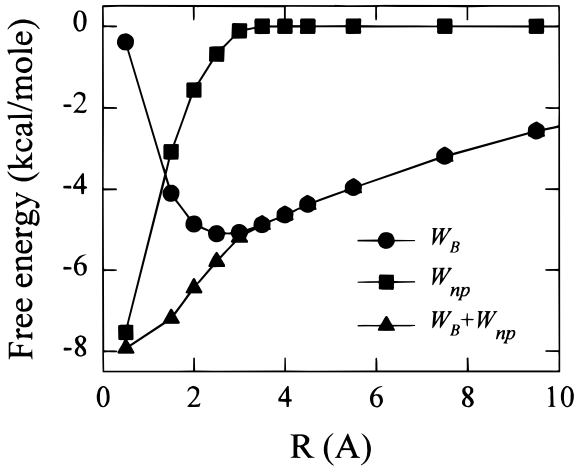


FIGURE 10: Electrostatic (●), nonpolar (■), and total (▲) free energies of interaction between nonmyr-Src(2−19) and a 2:1 PC/PS bilayer in 100 mM monovalent salt as a function of the distance, $R$, between the molecules' van der Waals surfaces. The peptide is oriented with respect to the membrane surface to optimize the electrostatic interaction; in Figure 2A, the membrane would be below and parallel to the peptide.

## NOTE ADDED IN PROOF

A paper on the EPR structural studies of myr-Src(2−19) by K. Victor and D. Cafiso, whose work is cited throughout this paper as a personal communication, has been accepted for publication (*78*).

## REFERENCES

1. Parsons, J. T., and Weber, M. J. (1989) *Curr. Top. Microbiol. Immunol. 147*, 79−127.
2. Resh, M. D. (1990) *Oncogene 5*, 1437−1444.
3. Brown, M. T., and Cooper, J. A. (1996) *Biochim. Biophys. Acta 1287*, 121−149.
4. Hunter, T. (1997) *Cell 88*, 333−346.
5. Buss, J. E., Kamps, M. P., and Sefton, B. M. (1984) *Mol. Cell. Biol. 4*, 2697−2704.
6. Schultz, A. M., Henderson, L. E., Oroszlan, S., Garber, E. A., and Hanafusa, H. (1985) *Science 227*, 427−429.
7. Deichaite, I., Casson, L. P., Ling, H. P., and Resh, M. D. (1988) *Mol. Cell. Biol. 8*, 4295−4301.
8. Resh, M. D. (1996) *Cell. Signalling 8*, 403−412.

9. Bhatnagar, R. S., and Gordon, J. I. (1997) *Trends Cell Biol. 7*, 14−21.
10. Kaplan, J. M., Varmus, H. E., and Bishop, J. M. (1990) *Mol. Cell. Biol. 10*, 1000−1009.
11. Sigal, C. T., Zhou, W., Buser, C. A., McLaughlin, S., and Resh, M. D. (1994) *Proc. Natl. Acad. Sci. U.S.A. 91*, 12253−12257.
12. Cross, F. R., Garber, E. A., Pellman, D., and Hanafusa, H. (1984) *Mol. Cell. Biol. 4*, 1834−1842.
13. Kamps, M. P., Buss, J. E., and Sefton, B. M. (1985) *Proc. Natl. Acad. Sci. U.S.A. 82*, 4625−4628.
14. Buss, J. E., Kamps, M. P., Gould, K., and Sefton, B. M. (1986) *J. Virol. 58*, 468−474.
15. Buser, C. A., Sigal, C. T., Resh, M. D., and McLaughlin, S. (1994) *Biochemistry 33*, 13093−13101.
16. Peitzsch, R. M., and McLaughlin, S. (1993) *Biochemistry 32*, 10436−10443.
17. McLaughlin, S., and Aderem, A. (1995) *Trends Biochem. Sci. 20*, 272−276.
18. Silvius, J. R., and l'Heureux, F. (1994) *Biochemistry 33*, 3014−3022.
19. Crothers, D. M., and Metzger, H. (1972) *Immunochemistry 9*, 341−357.
20. Perutz, M. (1990) *Mechanisms of Cooperativity and Allosteric Regulation in Proteins*, p 76, Cambridge University Press, Cambridge, U.K.
21. Hancock, J. F., Paterson, H., and Marshall, C. J. (1990) *Cell 63*, 133−139.
22. Ghomashchi, F., Zhang, X., Liu, L., and Gelb, M. H. (1995) *Biochemistry 34*, 11910−11918.
23. Page, M. I., and Jencks, W. P. (1971) *Proc. Natl. Acad. Sci. U.S.A. 68*, 1678−1683.
24. Honig, B. H., and Nicholls, A. (1995) *Science 268*, 1144−1149.
25. Honig, B. H., Sharp, K. A., and Yang, A. S. (1993) *J. Phys. Chem. 97*, 1101−1109.
26. Ben-Tal, N., Honig, B., Peitzsch, R. M., Denisov, G., and McLaughlin, S. (1996) *Biophys. J. 71*, 561−575.
27. Ben-Tal, N., Honig, B., Miller, C., and McLaughlin, S. (1997) *Biophys. J. 73*, 1717−1727.
28. Gould, K. L., Woodgett, J. R., Cooper, J. A., Buss, J. E., Shalloway, D., and Hunter, T. (1985) *Cell 42*, 849−857.
29. Walker, F., deBlaquiere, J., and Burgess, A. W. (1993) *J. Biol. Chem. 268*, 19552−19558.
30. Oude Weernink, P. A., and Rijksen, G. (1995) *J. Biol. Chem. 270*, 2264−2267.
31. Duronio, R. J., Towler, D. A., Heuckeroth, R. O., and Gordon, J. I. (1989) *Science 243*, 796−800.
32. Kim, J., Mosior, M., Chung, L. A., Wu, H., and McLaughlin, S. (1991) *Biophys. J. 60*, 135−148.
33. Fromherz, P. (1975) *Rev. Sci. Instrum. 46*, 1380−1385.
34. Boguslavsky, V., Rebecchi, M., Morris, A. J., Jhon, D. Y., Rhee, S. G., and McLaughlin, S. (1994) *Biochemistry 33*, 3032−3037.
35. Seelig, A. (1987) *Biochim. Biophys. Acta 899*, 196−204.
36. Barenholz, Y., Gibbes, D., Litman, B. J., Goll, J., Thompson, T. E., and Carlson, R. D. (1977) *Biochemistry 16*, 2806−2810.
37. Picard, D., and Yamamoto, K. R. (1987) *EMBO J. 6*, 3333−3340.
38. Ausubel, F. M., Brent, R., Kingston, R. E., Moore, D. D., Sediman, J. G., Smith, J. A., and Struhl, K. (1987) *Current Protocols in Molecular Biology*, John Wiley and Sons, New York.
39. Resh, M. D., and Erikson, R. L. (1985) *J. Cell Biol. 100*, 409−417.
40. White, S. H., Wimley, W. C., and Ladokhin, A. S. (1998) *Methods Enzymol.* (in press).
41. Lemmon, M. A., Ferguson, K. M., and Schlessinger, J. (1996) *Cell 85*, 621−624.
42. Garcia, P., Gupta, R., Shah, S., Morris, A. J., Rudge, S. A., Scarlata, S., Petrova, V., McLaughlin, S., and Rebecchi, M. J. (1995) *Biochemistry 34*, 16228−16234.
43. Aveyard, R., and Haydon, D. A. (1973) *An Introduction to the Principles of Surface Chemistry*, Cambridge University Press, Cambridge, U.K.
44. McLaughlin, S. (1989) *Annu. Rev. Biophys. Biophys. Chem. 18*, 113−136.
45. Bockris, J. O., and Khan, S. U. M. (1993) *Surface Electrochemistry: A Molecular Level Approach*, Plenum Press, New York.
46. Langner, M., Cafiso, D., Marcelja, S., and McLaughlin, S. (1990) *Biophys. J. 57*, 335−349.
47. Peitzsch, R. M., Eisenberg, M., Sharp, K. A., and McLaughlin, S. (1995) *Biophys. J. 68*, 729−738.
48. Charifson, P. S., Hiskey, R. G., and Pedersen, L. G. (1990) *J. Comput. Chem. 11*, 1181−1186.
49. Brooks, B. R., Bruccoleri, R. E., Olafson, B. D., States, D. J., Swaminathan, S., and Karplus, M. (1983) *J. Comput. Chem. 4*, 187−217.
50. Xu, W., Harrison, S. C., and Eck, M. J. (1997) *Nature 385*, 595−602.
51. Mosior, M., and McLaughlin, S. (1992) *Biochim. Biophys. Acta 1105*, 185−187.
52. Tanford, C. (1991) *The Hydrophobic Effect: Formation of Micelles and Biological Membranes*, 2nd ed., Kreiger Publishing, Malabar, FL.
53. Marsh, D. (1997) *Biochim. Biophys. Acta 1286*, 183−223.
54. Cross, F. R., and Hanafusa, H. (1983) *Cell 34*, 597−607.
55. Nicholls, A., Sharp, K. A., and Honig, B. (1991) *Proteins 11*, 281−296.
56. Parsegian, A. (1969) *Nature 221*, 844−846.
57. Ben-Tal, N. (1995) *J. Phys. Chem. 99*, 9642−9645.
58. Zhou, W., Parent, L. J., Wills, J. W., and Resh, M. D. (1994) *J. Virol. 68*, 2556−2569.
59. Massiah, M. A., Starich, M. R., Paschall, C., Summers, M. F., Christensen, A. M., and Sundquist, W. I. (1994) *J. Mol. Biol. 244*, 198−223.
60. Hill, C. P., Bancroft, D. P., Christensen, A. M., and Sundquist, W. I. (1996) *Proc. Natl. Acad. Sci. U.S.A. 93*, 3099.
61. Roux, M., Neumann, J. M., Bloom, M., and Devaux, P. F. (1988) *Eur. Biophys. J. 16*, 267−273.
62. Shen, L., Bassolino, D., and Stouch, T. (1997) *Biophys. J. 73*, 2−20.
63. Roux, B., and Woolf, T. B. (1996) in *Biological Membranes: A Molecular Perspective from Computation and Experiment* (Merz, K. M., and Roux, B., Eds.) pp 555−587, Birkhauser, Boston.
64. Wimley, W. C., and White, S. H. (1996) *Nat. Struct. Biol. 3*, 842−848.
65. Yaciuk, P., Choi, J. K., and Shalloway, D. (1989) *Mol. Cell. Biol. 9*, 2453−2463.
66. Clark, E. A., and Brugge, J. S. (1993) *Mol. Cell. Biol. 13*, 1863−1871.
67. Liebenhoff, U., Brockmeier, D., and Presek, P. (1993) *Biochem. J. 295*, 41−48.
68. Moyers, J. S., Bouton, A. H., and Parsons, S. J. (1993) *Mol. Cell. Biol. 13*, 2391−2400.
69. Zang, Q., Lu, Z., Curto, M., Barile, N., Shalloway, D., and Foster, D. A. (1997) *J. Biol. Chem. 272*, 13275−13280.
70. Gould, K. L., and Hunter, T. (1988) *Mol. Cell. Biol. 8*, 3345−3356.
71. Liebenhoff, U., Greinacher, A., and Presek, P. (1994) *Cell. Mol. Biol. 40*, 645−652.
72. Sharp, K. A., and Honig, B. H. (1990) *Annu. Rev. Biophys. Biophys. Chem. 19*, 301−332.
73. Sharp, K. A., and Honig, B. H. (1990) *J. Phys. Chem. 94*, 7684−7692.
74. Roth, C. M., and Lenhoff, A. M. (1993) *Langmuir 9*, 962−972.
75. Efron, B., and Tibshirani, R. (1993) *An Introduction to the Bootstrap*, Chapman and Hall, New York.
76. Sitkoff, D., Ben-Tal, N., and Honig, B. (1996) *J. Phys. Chem. 100*, 2744−2752.
77. Sridharas, S., Nicholls, A., and Honig, B. (1992) *Biophys. J. 61*, A174.
78. Victor, K., and Cafiso, D. (1998) *Biochemistry* (in press).


BI972012B